Effective Structure Factor of Osmotically Deformed Nanoemulsions†

T. G. Mason,*,‡,§,|| S. M. Graves,‡ J. N. Wilking,‡ and M. Y. Lin⊥

Department of Chemistry and Biochemistry, Department of Physics and Astronomy, California NanoSystems Institute, University of California-Los Angeles, Los Angeles, California 90095, and Center for Neutron Research, National Institute of Standards and Technology, Gaithersburg, Maryland 20899

Received: January 9, 2006; In Final Form: March 20, 2006

Extreme osmotic compression of nanoemulsion droplets, achieved by ultracentrifugation, can create solidlike biliquid foams without causing significant droplet coalescence. Using small-angle neutron scattering (SANS), we probe the structure of a uniform silicone oil-in-water nanoemulsion stabilized by sodium dodecyl sulfate over a wide range of volume fractions, ϕ, up to and beyond the limit associated with maximal random jamming of spheres, $\phi_{MRJ} = 0.64$. Although some features in the structure can be understood at lower ϕ using simple predictions for hard spheres, the anionic repulsion and deformability of the droplet interfaces creates departures from these predictions at higher ϕ. For ϕ near and beyond ϕ_{MRJ}, the effective structure factor, S_{eff}, as a function of wavenumber, q, exhibits a primary peak that is subunity. We speculate that this striking feature is due to the deformation of the droplets into nonspherical shapes as the system begins to approach the limit of a random array of nanoscopic thin films, Plateau borders, and vertexes characteristic of a polyhedral foam.

Emulsions and foams have common structures[1]: emulsions are suspensions of deformable liquid droplets in another immiscible liquid; foams are suspensions of deformable gas bubbles in a liquid. In both systems, if the droplets or bubbles are concentrated enough to cause deformation by the application of an osmotic pressure, then their mechanical properties can change from viscous to elastic.[2,3] This arises because the concentrated droplets and bubbles pack, press against their neighbors, and deform as the osmotic pressure is increased. The application of a small shear strain does work against the interfacial tension, σ, and causes the packed droplets to deform, thereby creating additional interfacial area and storing energy. As the droplet or bubble volume fraction, ϕ, is increased from the dilute "wet" limit, the spheres are quenched into a disordered configuration reminiscent of a glass.[2,4] Above the maximally random jammed (MRJ) volume fraction of spheres,[5,6] $\phi_{MRJ} = 0.64$ (previously referred to as random close packing[7,8]), the droplets develop small facets where they "touch" their neighbors, yet preserve a thin film due to a short-range repulsive interaction between the interfaces that inhibits coalescence. As ϕ is further increased into the highly concentrated "dry" limit, the droplets or bubbles begin to resemble polyhedra with rounded vertexes, and in an inverse sense, the structure can be imagined as an interconnected network of thin films and Plateau borders[9] (triangular ridges that run along the edges of the polyhedra). Thus, the problem of understanding macroscopic physical properties, such as the shear modulus[3,10] or electrical conductivity,[11] of foams and emulsions is intimately related to the interfacial structure of these systems. In fact, it is impossible to predict the macroscopic mechanical properties of these systems without knowing the details of the interfacial structures at the microscopic and nanoscopic limits.[12]

Developing a complete understanding of the bulk structure of emulsions and foams as a function of ϕ has remained elusive for many reasons. Three-dimensional visualization of confined foams near glass walls using macrophotography[13,14] or confocal microscopy[15] has revealed the structure of the films, Plateau borders, and vertexes. However, due to the boundary conditions imposed by the walls, it is not clear that these structures represent the average bulk structure of random foam. Moreover, the gravitational drainage[16−18] and diffusive coarsening[19] of foams cause the bubbles to continuously deform and rearrange and the overall structure to evolve. Although drainage and coarsening of foams are interesting phenomena in their own right, they generally preclude a study of bulk static structures.

By contrast to foams, emulsions offer several important potential advantages for revealing the static structure. The droplets can be comprised of a liquid that is not only immiscible but nearly completely insoluble in the continuous phase. We distinguish between immiscibility and insolubility because there is a subtle, yet important, difference in what these terms imply. Immiscible liquids form two distinguishably separate liquid phases sharing a well-defined interface, yet, at equilibrium, it is still possible for each of these two liquid phases to contain relatively small quantities of dissolved molecules of the other liquid. The solubility governs the quantitative concentrations of the molecules of the minority species in the majority phase. For emulsions, the insolubility of droplet molecules in the continuous phase prevents rapid coarsening of the droplet size distribution by diffusive transport of these molecules, even through the thin films. Reducing the solubility can generally be achieved by raising the molecular weight of molecules comprising the dispersed phase. By contrast, for foams, the gas molecules inside the bubbles are generally small enough and soluble enough that they can still cause structural changes over the time scales of hours or days. The use of larger gas molecules

† Part of the special issue "Charles M. Knobler Festschrift".

* To whom correspondence should be addressed. E-mail: mason@chem.ucla.edu.

‡ Department of Chemistry and Biochemistry.

§ Department of Physics and Astronomy.

|| California NanoSystems Institute.

⊥ National Institute of Standards and Technology.

10.1021/jp0601623 CCC: $33.50
Published on Web 04/28/2006

can reduce the rate of coarsening in gaseous foams somewhat, yet this rate is still vastly larger than the extremely small rate that can be achieved by using highly insoluble liquids in emulsions. Next, gravitational draining in emulsions can essentially be eliminated by either density matching the dispersed and continuous phases or making the average droplet size so small that thermal fluctuations preclude draining, creaming, or settling over a period of many days. For typical oil−water density differences of about 0.05 g/cm^3, this thermally stabilized emulsion can be achieved with droplets having radii, a, of about a micrometer or less. In addition, microscale emulsions of monodisperse droplets can be made through hydrodynamic focusing of a liquid jet of the dispersed phase in microfluidic devices[20,21] and through micelle-induced depletion fractionation of polydisperse emulsions.[22,23]

Scattering from microscale model emulsions have not yielded a complete picture of the bulk structure as a function of ϕ. Initial light scattering studies have probed the structure of fractionated emulsions.[24,25] A central difficulty in measuring the wavenumber-dependent structure factor, $S(q)$, encountered initially is that the wavelength of light is close to the size of the droplets, leading to extreme multiple light scattering commonly observed as the white appearance of milk and mayonnaise. To overcome this, the refractive index of the oil droplets was matched with that of the continuous water phase using glycerol. Two measurements of $S(q)$ for disordered monodisperse emulsions at high concentrations in the glassy regime have been published: one at $\phi = 0.7$[24] and one at $\phi = 0.54$.[25] Both measurements reveal correlation peaks at $qa \approx \pi$ characteristic of nearest-neighbor correlations. Interestingly, the magnitude of the peak of S is lower at $\phi = 0.7$ than at $\phi = 0.54$, although this had not been noted in the latter publication. Due to the difficulty of these experiments and complications with properly interpreting the scattering from a shell of different refractive index near the droplet surfaces, no systematic measurements of $S(q,\phi)$ of disordered uniform emulsions have been reported from the dilute limit, through the glass transition, jamming transition, and toward the dry limit.

To fill this gap in the available scattering data, we have performed small-angle neutron scattering (SANS) on uniform nanoscale emulsions over a wide range of ϕ from $\phi = 0.005$ to $\phi = 0.72$. We have developed a microfluidic method to make bulk quantities of nanoscale emulsions, or "nanoemulsions", having droplet radii less than 100 nm.[26] For a poly(dimethylsiloxane) (PDMS) silicone oil-in-water emulsion stabilized by sodium dodecyl sulfate (SDS), the range of average droplet radii can be varied from several hundred nanometers down to about 10 nm using extreme shear and high surfactant concentration. The nanoemulsions are true metastable emulsions in the sense that they are produced from a top-down approach of rupturing larger oil droplets into smaller ones, not through a bottom-up approach, such as causing mutually soluble components to self-assemble into a lyotropic liquid crystalline phase of droplets. Due to the low solubility of the PDMS in the aqueous phase, Ostwald ripening[27] is negligible over months. After bulk production, the size distribution of the emulsions can be sharpened through a succession of ultracentrifugal fractionation steps.[26] The result is that uniform nanoemulsions can be obtained in quantities of tens of milliliters, sufficient for a complete structural study using SANS. Moreover, during the fractionation, D_2O can be substituted for H_2O thereby enhancing the scattering contrast and reducing SANS data collection times.

To measure the structure of monodisperse nanodroplets, we make a concentrated stock nanoemulsion at $\phi = 0.72$ and 10 mM SDS in D_2O. To obtain lower ϕ, we dilute this stock emulsion with a surfactant solution identical to that of the continuous phase: 10 mM SDS in D_2O. This approach keeps the ionic strength and neutron scattering length density constant for all measurements, so that changes in intensity are due primarily to changes in ϕ and not changes in the droplet interaction potential or scattering contrast. After the SDS solution is added, the emulsions are stirred and allowed to equilibrate for at least 8 h to ensure a homogeneous ϕ everywhere in the sample. The liquidlike samples at dilute ϕ are loaded into banjo cells of 1 mm path length, and the solidlike samples at higher ϕ are loaded into demountable cells having a spacer that can be controlled from 0.1 to 1 mm. We measure the transmission prior to collecting the wavenumber-dependent intensity, $I(q)$. Due to the significant scattering contrast and nanoscale droplet size, multiple scattering can occur in the most concentrated samples. If the transmission indicated that greater than 10% of the neutrons had been scattered more than once, then we reduced the spacer thickness until we measured a transmission that met this criterion. Even at a cell thickness of 0.1 mm, the distance between the cell's windows is more than 1000 times the droplet radius, thus ensuring a bulk measurement of the structure of random monodisperse droplets. All of our measurements are performed at a temperature of $T = 24$ °C and a neutron wavelength of $\lambda = 8$ Å. The neutron scattering length densities for the components we use, in units of 10^{10} cm^{-2}, are 6.41 (D_2O), −0.255 (PDMS), and 0.455 (SDS). We employ high and low q detector configurations that overlap to obtain a very large, effective q range. Incoherent neutron scattering is negligible for the range of q and ϕ that we consider.

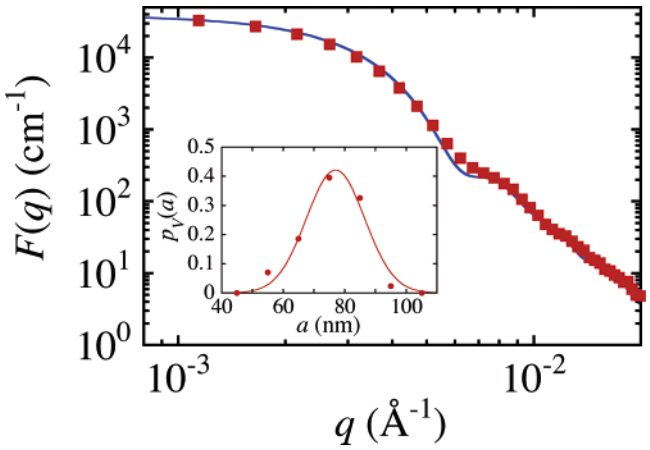

Figure 1. Measured SANS intensity of a silicone oil-in-water emulsion at a dilute droplet volume fraction $\phi = 0.005$ provides the wavenumber-dependent form factor, $F(q)$. The solid line is a regularized fit using a monomodal size distribution of spheres. Inset: the relative volume-weighted probability as a function of droplet radius, a, determined from the regularized fit; a simple Gaussian fit (line) yields an average radius $\langle a \rangle = 77$ nm and standard deviation $\delta a = 10$ nm.

We have characterized the structure of a dilute nanoemulsion to obtain information about the average size and polydispersity. In Figure 1, we show the form factor, $F(q)$, of the nanoemulsion at $\phi = 0.005$. This form factor is related to the Fourier transform of the shape of a sphere and would exhibit peaks and sharp minima as the intensity drops toward higher q if the sample had been perfectly monodisperse.[28] Even after fractionation, some polydispersity remains in the size distribution, as evidenced by the shallow minima and rounded secondary shoulder that appears at higher q. By fitting the form factor using a regularization method that varies the weights of contributions to the intensity from droplets having different sizes, we obtain the solid line in Figure 1. Overall, the fit agrees well with the

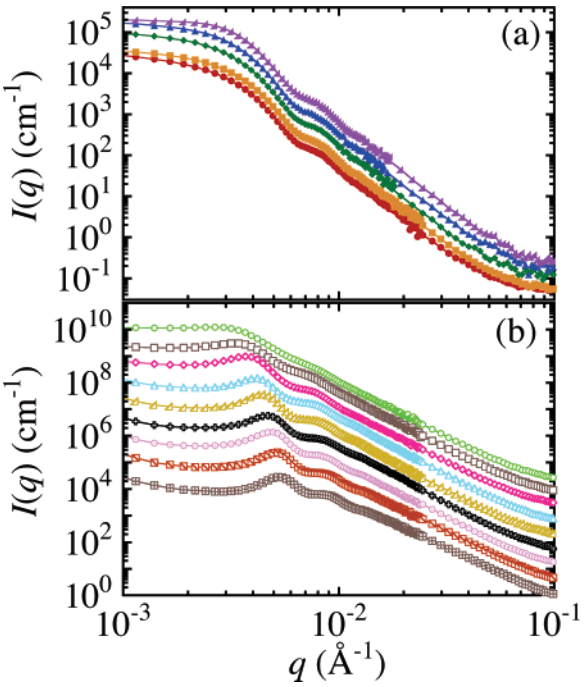

Figure 2. Measured SANS intensity, I, as a function of wavenumber, q, of the nanoemulsion as ϕ is increased: (a) $\phi = 0.005$, 0.009, 0.021, 0.043, and 0.085 (from bottom to top); (b) $\phi = 0.17$, 0.24, 0.32, 0.39, 0.45, 0.52, 0.60, 0.67, and 0.72 (from top to bottom). In part b only, all $I(q)$ values for $\phi < 0.7$ have been shifted vertically by a factor of 5 in succession to facilitate viewing.

data, and the weights determined by the fit are shown in the inset. The droplet size distribution is monomodal, having a volume-weighted average radius of $\langle a \rangle = 77$ nm and a standard deviation of $\delta a = 10$ nm. This standard deviation actually represents an upper bound, since the incident neutrons have a wavelength spread, $\Delta\lambda/\lambda = 0.1$, that is smaller than the polydispersity $\delta a/\langle a \rangle = 0.13$. Although the droplets are quite uniform in size, this residual polydispersity is still above the crystallization limit of hard spheres at about $\delta a/\langle a \rangle \approx 0.06$[29,30] and ensures that the droplet positional structure remains disordered at all ϕ.

To systematically probe the changes in the structure of disordered deformable nanodroplets from the dilute to the concentrated limit, we have measured $I(q,\phi)$ for $0.005 \leq \phi \leq 0.72$, as shown in Figure 2. As ϕ is increased from the very dilute limit, the intensity increases proportional to ϕ and only small changes in the shape of $I(q)$ can be seen at the lowest ϕ (see Figure 2a). Additional increases in ϕ lead to the appearance of a noticeable peak in $I(q)$ above about $\phi \approx 0.2$ as the intensity at low q is further suppressed (see Figure 2b). Moreover, the secondary shoulder at higher q becomes more pronounced. At yet larger $\phi > 0.5$, the overall intensity at low q, including the intensity of the primary peak and secondary shoulder, drops.

To emphasize changes in the shape of $I(q)$ compared with $F(q)$, we scale $F(q)$ upward until it matches $I(q)$ at high $q = 0.03$ Å^{-1}, and co-plot the results for several ϕ values in Figure 3. The scaling factor is essentially ϕ divided by the volume fraction of 0.005 at which the form factor measurement has been made. Making this comparison is sensible because correlation effects in the scattering that may be present at lower q should not be seen at higher q, so the shape of coherent scattering in both $I(q)$ and $F(q)$ should be the same at high q. For $\phi = 0.24$, the low q intensity is suppressed since droplets cannot interpenetrate with their neighbors and a very slight peak is present at intermediate q. The right-hand side of the peak matches the

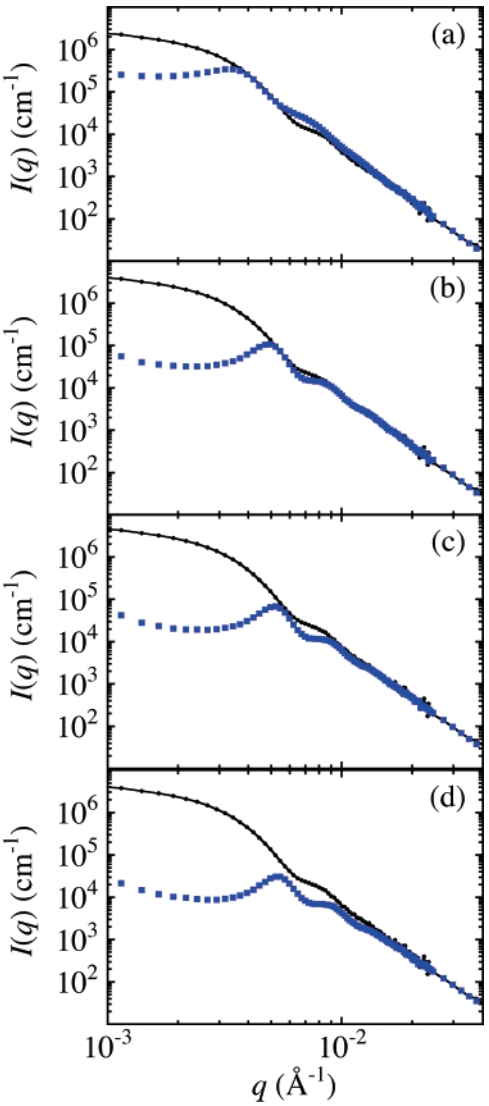

Figure 3. Comparison of SANS intensity as a function of wavenumber, $I(q)$, of concentrated nanoemulsions (squares) with the form factor, $F(q) = I(q, \phi \rightarrow 0)$, which has been scaled upward so that both overlap at high q values (small points and line): (a) $\phi = 0.24$, (b) $\phi = 0.60$, (c) $\phi = 0.67$, and (d) $\phi = 0.72$.

form factor, and the secondary shoulder rises above that of the form factor at intermediate q. At the highest ϕ, the peak is much more pronounced and both the peak and the shoulder lie completely below the rescaled form factor (see Figure 3d). In all of the measured $I(q)$, there is a small upturn in I at the lowest q; this very minor feature is indicative of a small amount of residual scattering from a few large droplets that might have been created due to droplet coalescence during the sample handling.

The reduction in the intensity at low q in nanoemulsions is reminiscent of that observed for impenetrable hard spheres. In Figure 4, we compare the intensity, $I_L(\phi)$, at the lowest q we probe with the Percus−Yevick (PY) hard sphere (HS) structure factor for disordered monodisperse spheres,[31] S_{HS}, multiplied by the droplet volume fraction: $I_{HS}(\phi, q \rightarrow 0) \sim \phi S_{HS}(\phi)$. Overall, there is good agreement for $\phi \leq 0.495$, the volume fraction associated with the disorder−order transition below which the PY−HS theory is expected to be a good approximation. Above this volume fraction, the scattering intensity from nanoemulsions lies above the hard sphere prediction. This deviation is not surprising at the highest ϕ, since the droplets are undoubtedly deformed.

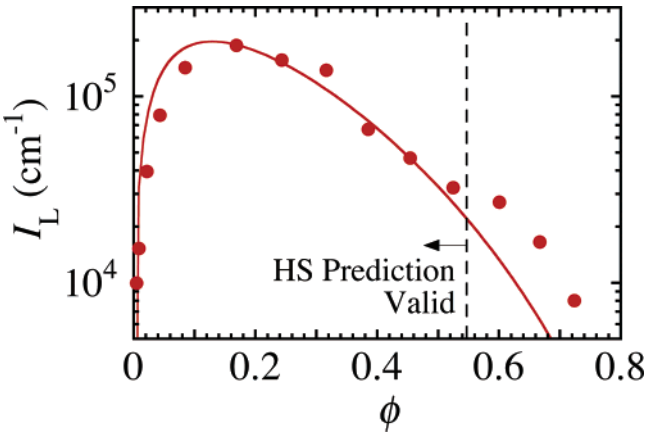

Figure 4. Volume fraction dependence of the low wavenumber intensity, $I_L(\phi)$, of nanoemulsions from the dilute to the concentrated regime. The solid line is a prediction for disordered monodisperse Percus−Yevick hard spheres expected to be valid below the known crystallization volume fraction of $\phi_{X-HS} = 0.545$ (dashed line).

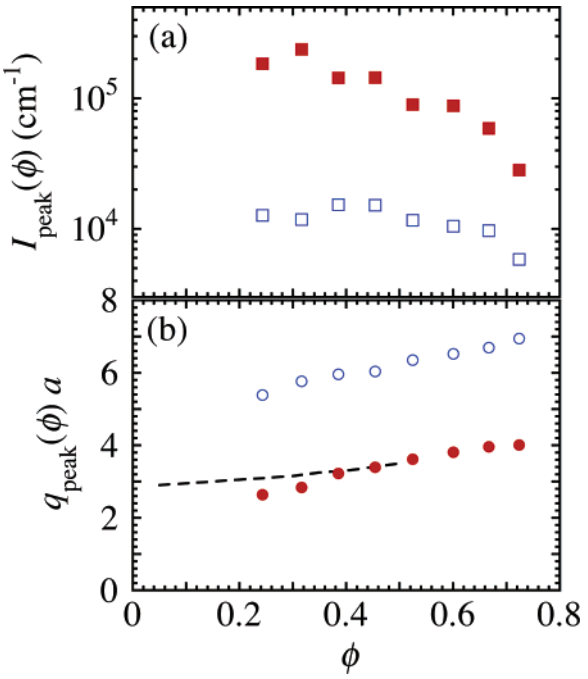

Figure 5. Volume fraction dependence of (a) the intensity, $I_{peak}(\phi)$, associated with the primary (solid squares) and secondary (open squares) peaks in $I(q)$; (b) the dimensionless wavenumber, $q_{peak}(\phi)a$, associated with the primary (solid circles) and secondary (open circles) peaks in $I(q)$. The dashed line is the prediction for monodisperse hard spheres based on the Percus−Yevick closure.

The positions and intensities associated with the primary peak and secondary shoulder are shown as a function of volume fraction in Figure 5. We focus on the behavior of the primary peak, since it captures information about nearest-neighbor correlations. For $\phi > 0.3$, the peak intensity, I_{peak}, drops as ϕ of the nanoemulsions is raised. By contrast, for dispersions of hard spheres, one would expect the peak intensity to continue to increase as the droplet volume fraction is raised toward the MRJ limit.[31] The dimensionless wavenumber associated with the peak, $q_{peak}a$, is very similar to what one would expect from hard spheres (see dashed line in Figure 5b); the peak occurs at an interdroplet separation that is about equal to the diameter of an undeformed droplet, so $q_{peak}a \approx \pi$.

To illustrate the unusual features of the scattering from concentrated nanoemulsions, we calculate an effective structure factor, S_{eff}, by dividing the measured intensity by the rescaled form factor, taken from Figure 3. The results for the three highest droplet volume fractions are shown in Figure 6. Strikingly, for $\phi \geq 0.60$, the primary nearest-neighbor correlation peaks in $S_{eff}(q)$ lie at or below unity. This unusual behavior indicates that some very interesting changes in the structure occur when nanoemulsions are concentrated to high ϕ.

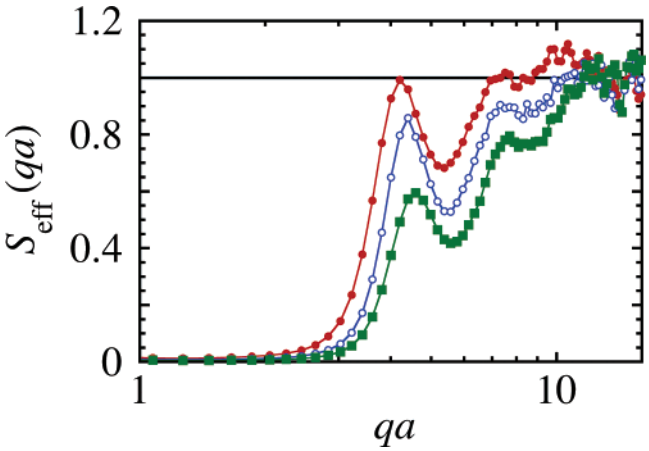

Figure 6. Effective structure factor, S_{eff}, as a function of dimensionless wavenumber, qa, at highly concentrated volume fractions: $\phi = 0.60$ (solid circles), 0.67 (open circles), and 0.72 (solid squares). To obtain $S_{eff}(q)$, $I(q)$ is divided by the rescaled form factor $F(q)$, shown in Figure 3. Subunity peaks in S_{eff} are clearly visible at the highest ϕ. At high q values, the data trend toward the expected limit, $S_{eff} = 1$ (heavy solid line).

The structure factor that we have calculated is "effective" in the sense that we apply the division operation blindly; this is tantamount to assuming that the droplet shape does not change at high ϕ. Theoretically, the separation of the total scattered intensity into the product of the structure factor and the form factor, $I(q,\phi) = S(q,\phi)F(q)$, is valid only when the shape of the scattering objects does not change. For nanoemulsion droplets that can deform at high ϕ, there is no guarantee that $F(q)$ properly captures the shape, so S_{eff} that we have calculated could also contain information about the shape changes of the droplets as well as information about relative interdroplet positional correlations. Although the droplets may develop facets and rounded edges as they are concentrated, their volumes must remain constant, so the average form factor of a deformed droplet is not far from that of a perfect sphere. The decrease in the value of the primary peak of $S_{eff}(\phi)$ toward larger ϕ is similar to our prior observations on a slightly more polydisperse nanoemulsion that had not been as highly concentrated.[32] Moreover, the peaks in our SANS data clearly arise from nanodroplet structures; this is in contrast to the peaks due to micellar structures seen in SANS studies of foams[33] comprised of 100−300 μm bubbles stabilized by SDS at concentrations significantly larger than 10 mM.

One contributing factor to the subunity peaks in $S_{eff}(q)$ is due to the overall increase in the surface-to-volume ratio of interfaces in the nanoemulsion as the droplets are concentrated. Neutrons scattered from random structures having interfaces that exhibit a step change in the neutron scattering length density across the interface give rise to the well-known Porod scattering law:[34] $I(q) \sim (A/V)q^{-4}$ valid at high $q \gg A/V$, where A/V represents the surface area-to-volume ratio of the objects with interfaces. For nanoemulsions comprised of deformed droplets at high ϕ, the intensity does indeed follow q^{-4}, yet the ratio A/V will be larger at high q than it would have been if the droplets had remained undeformed, thereby increasing the intensity somewhat

beyond what would be expected just from the increase in droplet density. Since the intensity at high q is shifted upward from this effect, the matching of the form factor there and the subsequent division leaves the peak values of S_{eff} below unity. Thus, we believe that part of the explanation for this unusual feature in S_{eff} can be attributed to droplet deformation and extra (A/V) present at high q when the emulsion is osmotically compressed.

A simulation of random monodisperse foam[35] contains a quantitative estimate of the increase in surface area per bubble from a wet foam of spherical bubbles to a dry foam of polyhedral bubbles. The increase in surface area per bubble, on average, is only about 10%. Although this increase is in the correct direction and helps to partially explain the subunity peaks in $S_{eff}(q)$, it certainly does not account for the much more substantial reduction in intensities that we have observed in osmotically compressed emulsions at low q. Another source that could contribute to the suppression of the peak intensity at high ϕ could be due to a less-regular positional arrangement of neighboring droplets into correlation shells as the droplet deformation becomes more extreme. However, this effect is expected to be minor compared with the increased surface-to-volume ratio effect that alters the magnitude of $I(q)$ at high q where it is matched with $F(q)$ to determine the structure factor.

In addition to droplet deformation, polydispersity in the size distribution and screened repulsive interactions between the charged droplets play a role in the shape of the measured intensities. The movement of the secondary shoulder in $I(q)$ above the shoulder of the rescaled form factor in Figure 3a could be partially due to enhanced interdroplet correlations that are more apparent above the dilute limit in ϕ; these positional correlations become more obvious at higher ϕ despite the residual polydispersity which causes more smearing of the shoulder in the form factor. The screened charge repulsions between the droplets are short in range, since the Debye screening length at a monovalent ionic strength of 10 mM is roughly $\lambda_D = 3$ nm. Although this is small relative to the average droplet radius of 77 nm, it implies that the droplets essentially "touch" at center-to-center separations larger than $2\langle a\rangle$. Assuming the droplets remain spherical, the effective volume fraction can be estimated as[3]: $\phi_{eff} \approx \phi(1 + \lambda_D/\langle a\rangle)^3$; for the nanoemulsion used in this experiment, $\phi_{eff} \approx 1.13\phi$. Thus, it is reasonable to argue that the highest volume fraction we probe in terms of packing considerations is closer to $\phi_{eff} = 0.81$. Although this is still far from the dry polyhedral foam limit, nevertheless, screened interfacial repulsions place our highest ϕ_{eff} well into the deformed droplet regime. We speculate that the effective structure factor of nanoemulsions, if corrected for the enhanced effects of the interfacial repulsions and the increased Porod scattering at high q due to droplet deformation, would resemble the structure factor previously observed using light scattering on index-matched microscale droplets. These corrections would cause the correlation peaks to rise above unity.

We believe that these measurements and interpretations are fundamentally interesting and important for several reasons. Our SANS measurements themselves represent a key systematic scattering study of the ensemble-averaged structure of disordered deformable uniform objects that maintain constant volume and minimize the interfacial area as an osmotic compression is applied. They clearly show the crossover from the dilute limit, where the screened repulsive droplets resemble hard spheres to a good approximation, to the compressed limit, where the droplets are deformed as they press against their neighbors. The approach of making uniform nanoemulsions to match the accessible q range of the SANS technique has overcome significant obstacles created by multiple scattering that complicates light scattering methods. Thus, this study represents a thorough systematic exploration of the structural crossover between a wet biliquid foam of disordered undeformed spherical droplets at low ϕ and a concentrated biliquid foam of significantly deformed droplets at high ϕ.

Although the structure of hard spheres can be used to explain the features in $I(q,\phi)$ at low q, this approach fails when considering the behavior of the peaks and shoulders at higher q as ϕ is increased. In this limit, no theories or simulations are available that predict the ensemble-averaged structure of random disordered emulsions or foams as the droplets or bubbles are concentrated from the effective packing limit into the dry limit. To explain all of the features we have measured, the theory or simulation would have to self-consistently minimize the sum of the interfacial energy associated with deformation plus the interaction energy associated with the screened repulsion between the charged interfaces. All of this must be done while keeping the droplet volumes fixed and the droplet positional structure in a quenched disordered configuration. To produce such a simulation would be a very large step forward in the field of foams and emulsions, and it would enable us to compare our ensemble-averaged structure factors with those calculated from interfacial structures simulated in real space. However, making a simulation having this complexity would be no easy task; including the effects of polydispersity would only add to this complexity. Unfortunately, our scattering measurements are not at large enough ϕ to directly compare with very nice recent simulations of random monodisperse foams in the dry limit.[35,36] We believe that it may be possible to address the structure at very large ϕ theoretically by considering a randomly oriented array of Plateau borders and thin films of relatively uniform length and area, respectively, that have spacings roughly separated by $2\langle a\rangle$. If the volume of the continuous phase is held mostly in the Plateau borders, then we anticipate that the scattering intensity in this limit will closely resemble what would be obtained for porous solid foams.

In the future, we will attempt to osmotically compress nanoemulsions to an even larger extent to see if we can reach the dry limit without encountering significant problems with droplet coalescence. By further reducing the droplet polydispersity through additional fractionation steps, we will attempt to make concentrated colloidal crystals of deformable nanoscale droplets. Contrast variation experiments using different ratios of H_2O/D_2O in the continuous phase may also shed light on the possible role of the surfactant on the effective structure factor. These are among the interesting frontiers that remain to be explored in the emerging science of nanoemulsions.

Acknowledgment. T.G.M. thanks Prof. Chuck Knobler for many interesting and stimulating discussions about nanoemulsions and about the physical chemistry of interfaces and dispersions. We also thank Prof. John McTague for supporting this work financially.

References and Notes

(1) Bibette, J.; Leal-Calderon, F.; Poulin, P. *Rep. Prog. Phys.* **1999**, *62*, 969.

(2) Mason, T. G.; Bibette, J.; Weitz, D. A. *Phys. Rev. Lett.* **1995**, *75*, 2051.

(3) Mason, T. G.; Lacasse, M.-D.; Grest, G. S.; Levine, D.; Bibette, J.; Weitz, D. A. *Phys. Rev. E* **1997**, *56*, 3150.

(4) van Megen, W.; Underwood, S. M. *Phys. Rev. E* **1994**, *49*, 4206.

(5) Liu, A. J.; Nagel, S. R. *Nature* **1998**, *396*, 21.

(6) Donev, A.; Cisse, I.; Sachs, D.; Variano, E. A.; Stillinger, F. H.; Connelly, R.; Torquato, S.; Chaikin, P. M. *Science* **2003**, *303*, 990.
(7) Berryman, J. G. *Phys. Rev. A* **1983**, *27*, 1053.
(8) Bernal, J. D.; Mason, J. *Nature* **1960**, *188*, 910.
(9) Becher, P. *Emulsions: Theory and Practice*; Reinhold: New York, 1965.
(10) Gopal, A. D.; Durian, D. J. *Phys. Rev. Lett.* **2003**, *91*, 188303.
(11) Feitosa, K.; Marze, S.; Saint-Jalmes, A.; Durian, D. J. *J. Phys.: Condens. Matter* **2005**, *17*, 6301.
(12) Mason, T. G. *Curr. Opin. Colloid Interface Sci.* **1999**, *4*, 231.
(13) Hutzler, S.; Peron, N.; Weaire, D.; Drenckham, W. *Eur. Phys. J. E* **2004**, *14*, 381.
(14) Reinelt, D. A.; Boltenhagen, P.; Rivier, N. *Eur. Phys. J. E* **2001**, *4*, 299.
(15) Koehler, S. A.; Hilgenfeldt, S.; Weeks, E. R.; Stone, H. A. *Phys. Rev. E* **2002**, *66*, 040601.
(16) Stone, H. A.; Koehler, S. A.; Hilgenfeldt, S.; Durand, M. *J. Phys.: Condens. Matter* **2003**, *15*, S283.
(17) Hilgenfeldt, S.; Koehler, S. A.; Stone, H. A. *Phys. Rev. Lett.* **2001**, *86*, 4704.
(18) Hilgenfeldt, S.; Kraynik, A. M.; Koehler, S. A.; Stone, H. A. *Phys. Rev. Lett.* **2001**, *86*, 2685.
(19) Durian, D. J.; Weitz, D. A.; Pine, D. J. *Science* **1991**, *252*, 686.
(20) Anna, S. L.; Bontoux, N.; Stone, H. A. *Appl. Phys. Lett.* **2003**, *82*, 364.
(21) Dreyfus, R.; Tabeling, P.; Williame, H. *Phys. Rev. Lett.* **2003**, *90*, 144505.
(22) Bibette, J.; Roux, D.; Nallet, F. *Phys. Rev. Lett.* **1990**, *65*, 2470.
(23) Asakura, S.; Oosawa, F. *J. Chem. Phys.* **1954**, *22*, 1255.
(24) Mason, T. G.; Krall, A. H.; Gang, H.; Bibette, J.; Weitz, D. A. Monodisperse Emulsions: Properties and Uses. In *Encyclopedia of Emulsion Technology*; Becher, P., Ed.; Marcel Dekker: New York, 1996; Vol. 4, p 299.
(25) Gang, H.; Krall, A. H.; Cummins, H. Z.; Weitz, D. A. *Phys. Rev. E* **1999**, *59*, 715.
(26) Meleson, K.; Graves, S.; Mason, T. G. *Soft Mater.* **2004**, *2*, 109.
(27) Taylor, P. *Adv. Colloid Interface Sci.* **2003**, *106*, 261.
(28) Johnson, C. S.; Gabriel, D. A. *Laser Light Scattering*; Dover: New York, 1981.
(29) Pusey, P. N. *J. Phys.* **1987**, *48*, 709.
(30) Pusey, P. N.; vanMegen, W. *Nature* **1986**, *320*, 340.
(31) Ashcroft, N. W.; Lekner, J. *Phys. Rev.* **1966**, *145*, 83.
(32) Graves, S.; Meleson, K.; Wilking, J.; Lin, M. Y.; Mason, T. G. *J. Chem. Phys.* **2005**, *122*, 134703.
(33) Alexos, M. A. V.; Boue, F. *Langmuir* **2003**, *19*, 6598.
(34) Mildner, D. F. R.; Hall, P. L. *J. Phys. D: Appl. Phys.* **1986**, *19*, 1535.
(35) Kraynik, A. M.; Reinelt, D. A.; van Swol, F. *Phys. Rev. Lett.* **2004**, *93*, 208301.
(36) Kraynik, A. M.; Reinelt, D. A.; van Swol, F. *Phys. Rev. E* **2003**, *67*, 031403.